(Received 14 December 2023, Accepted 18 January 2024, Scheduled 9 March 2024)

Broadband Bowtie-Based Log-Periodic Array Antenna via GIPD Process for 5G mm-Wave Applications

Jixuan Li*, Zenghui Xiang, Xuan Chen, Mi Xu, and Jinhui Li

Information & Telecommunication Branch, State Grid Jiangsu Electric Power CO., LTD, Nanjing, China

ABSTRACT: In this paper, a broadband bowtie-based log-periodic array antenna is proposed and investigated for 5G millimeter wave (mm-wave) applications. Using a Glass Integrated Passive Device (GIPD) process the proposed antenna is implemented on a high dielectric constant glass substrate. To address the directional radiation issues associated with the traditional straight connection, the proposed antenna uses a crisscross connection effect with carefully spaced three dipole elements. Furthermore, the use of bowtie-based dipole offers a wide bandwidth advantage. The study also examines the effects of changes in key parameters on critical antenna features. The feeding structure uses a combination of coplanar waveguide (CPW) and microstrip line to strip line. For demonstration, a prototype antenna is optimized, fabricated, and measured. The measurement results show that the 10 dB impedance bandwidth of the proposed antenna is from 21.5 to 36.1 GHz, and the gain is higher than 5.63 dBi.

1. INTRODUCTION

Due to its natural characteristics, such as wide bandwidth, high data rates, and strong directional characteristics, millimeter-wave (mm-wave) technology has significantly contributed to the advancement of fifth-generation (5G) mobile communication technology [1, 2]. The 3GPP Release 15 standard has defined the n257, n258, and n261 5G-NR FR2 bands for 5G mm-wave communication applications [3]. These frequency bands offer advantages such as high-speed data transfer, low-latency communication, and coverage in densely populated urban areas. They are suitable for various applications, including data centers, cloud computing, the Internet of Things (IoT), the Internet of Vehicles, remote healthcare, and industrial automation [4–7].

The dielectric properties have a significant impact on the performance of millimeter-wave antennas. With its stable dielectric constant and low loss, glass serves as an ideal substrate due to its advantages in integration, accuracy, stability, and surface finish [8]. It is well suited for the use in portable and mobile devices and can withstand harsh weather conditions during operation. When being seamlessly integrated into structures such as windows and displays, the glass antennas enhance millimeter-wave signal transmission without altering the appearance, thus overcoming the challenges of signal loss and obstruction. In addition, glass is a cost-effective and widely used material that shows promise for achieving efficient and cost-effective mm-wave communication in 5G networks.

Recently, several 28 GHz antennas utilizing a glass substrate have been demonstrated to enhance reliability and decrease fabrication complexity and cost [9–15]. In [9], a 28 GHz Yagi-Uda antenna is designed, achieving a measured gain exceeding 3.44 dBi with a relative bandwidth of over 28.2%. In [10], a broadband 28 GHz on-glass end-fire array for 5G handsets is proposed, demonstrating a simulated relative bandwidth of 11.3% and a gain ranging from 7.08 to 8.36 dBi across the operating band. In [11], a planar quasi Yagi-Uda antenna utilizing liquid crystal (LC) technology is presented. The antenna is constructed on the inner surfaces of two parallel glass substrates with a thin LC layer filled in the feed section, demonstrating a measured bandwidth of 31%, a front-to-back ratio exceeding 15 dB, and a gain of 9.0 dBi at 28 GHz. Using the resin fan-out package process, a slot-coupled antenna is designed on a glass wafer for 5G IoT communication. The simulated bandwidth ranges from 27.8 to 28.7 GHz with a gain of 5.91 dB at 28 GHz [12]. In [13], a printed 5G monopole antenna with a periodic patch director on the laminated window glass is proposed for autonomous vehicle applications. The monopole antenna features a wide impedance bandwidth that covers the n257 band with a maximum gain of 1 dBi at 28.75 GHz. In [14], a square loop right hand circularly polarized (RHCP) antenna is designed by adopting a multi-layer glass wafer. The antenna is fed by two T-shaped patches through adjacent coupling, resulting in a fabricated 4×4 antenna array with a wide impedance bandwidth of 23–28 GHz and an RHCP gain of 5 dBi. In [15], a 1×4 series-coupled patch array antenna is implemented on a low-loss glass substrate using a single through glass via (TGV) for 28 GHz mm-wave wireless communication applications. The proposed antenna displays a considerable impedance bandwidth from 27.8 GHz to 28.9 GHz, featuring a realized peak gain of 10 dBi. Unfortunately, these existing glass antennas exhibit insufficient performance to wholly support n257, n258, and n261 band applications.

To solve this problem, based on the GIPD process, this work proposes a 28 GHz broadband bowtie-based log-periodic array antenna for 5G mm-wave applications. To overcome the chal-

* Corresponding author: Jixuan Li (lixuanji2023@163.com).

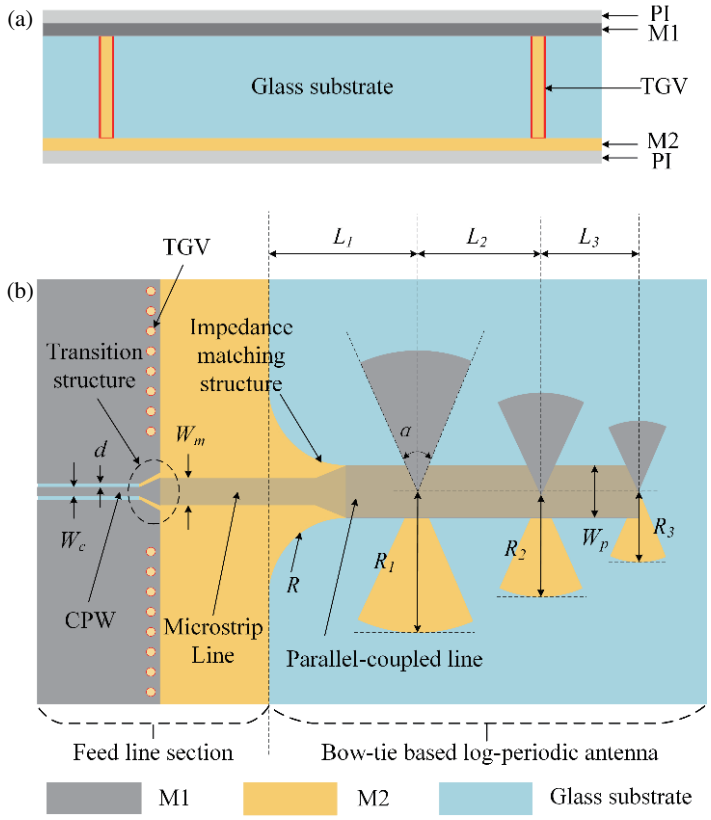

FIGURE 1. (a) Stack-up of the antenna substrate. (b) Top view of the proposed antenna.

lenges associated with conventional straight connections and their effects on radiation direction, the proposed antenna strategically arranges three dipole elements. This arrangement creates a cross-connection effect. In addition, to achieve wide bandwidth, the bowtie-based dipole is adopted and optimized for wide bandwidth performance. In addition, the CPW to microstrip line structure and microstrip line to strip line structure are introduced to feed the antenna. The overall size of the proposed antenna is $1.12 \times 0.65\lambda^2$ (where λ is the free-space wavelength at 28 GHz). Measurement results show that the antenna has excellent performance, which will meet the requirements of 5G mm-wave applications.

This paper is organized as follows. Section 2 shows the geometry of the proposed antenna. In Section 3, the operating principle and parametric analysis of the antenna are discussed. Section 4 presents simulation and measurement results of the proposed antenna. Finally, a conclusion is given in Section 5.

2. GEOMETRY OF THE PROPOSED ANTENNA

Figure 1(a) presents a simplified cross-section view of the proposed antenna layers. The main substrate utilized in this design is the alkali-free AF32 glass produced by SCHOOT technology, which offers tight geometric tolerances and a low Coefficient of Thermal Expansion (CTE) of 3.2. According to [16], the substrate possesses a relative dielectric constant and loss tangent of 5.1 and 0.0069 at 24 GHz, respectively. A trade-off is observed between performances in terms of radiation efficiency and bandwidth, determined by a thickness of $h_1 = 300\,\mu$m, corresponding to $0.028\lambda_0$ (where λ_0 is the wavelength in free space at 28 GHz). The radiation element and its feeding network are formed by two conductive layers, M1 and M2, utilizing electroplated copper of 5 µm thickness on the substrate surfaces. Through glass via (TGV) technique is employed, utilizing a via/land size of 50/110 µm. To prevent oxidation of the metal, both the M1 and M2 layers are coated with a polyimide (PI) layer with a dielectric constant of 3.2, a loss tangent of 0.001, and a 10 µm thickness.

Figure 1(b) shows the top view of the proposed log-periodic antenna based on a bowtie design. The antenna comprises two sections: 1) middle bowtie-based log-periodic antenna and 2) feed line structure. The middle bowtie-based log-periodic antenna in this design includes three circular bowtie elements with an equal flare angle α and parallel-coupled lines with a width W_p. The dipoles are symmetrically printed on the M1 and M2 layers. As shown in Fig. 1 (b), each arm of the dipoles on one side is connected to the parallel-coupled lines with a spacing of L_2 and L_3, and L_2/L_3 is set to u. The radii of the three elements are R_1, R_2, and R_3, and $R_1/R_2 = R_2/R_3 = v$. For wideband impedance matching, a transition structure from parallel-coupled lines to microstrip lines is designed. The width of the ground plane is symmetrically tapered by quarter circles of radius R between the parallel-coupled lines and the microstrip line to achieve the transition. Furthermore, the microstrip line ground functions as a reflector. A transition structure from a microstrip line to CPW line is introduced in the feed line section

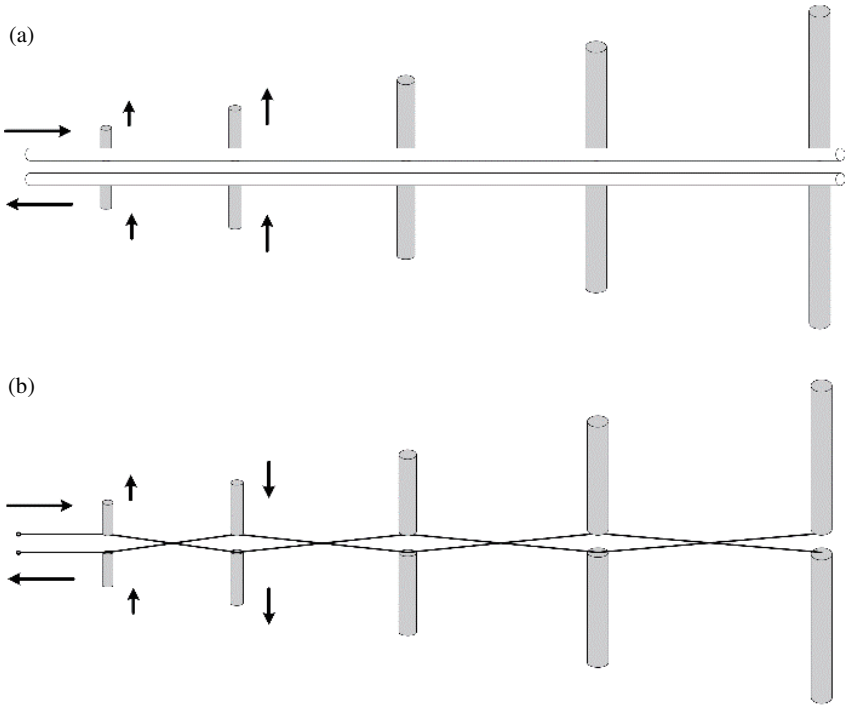

FIGURE 2. Basic connection types. (a) Straight connection. (b) Crisscross connection.

to facilitate testing or packaging of the antenna with Ground-Signal-Ground (GSG) probes.

3. OPERATING PRINCIPLE AND PARAMETRIC ANALYSIS OF THE ANTENNA

Typically, there are two basic connection types for feeding the elements of a log-periodic dipole array, as shown in Fig. 2 [17]. Fig. 2(a) illustrates the straight feed with close spacing and phase alignment, which potentially reduces the difficulty of the antenna design and fabrication. However, this configuration can introduce detrimental interference effects due to phase progression, which can distort the radiation pattern. To address this issue, as shown in Fig. 2(b), a 180-degree phase inversion at the end of each element is employed, which is achieved by mechanically alternating the feed between adjacent elements. This strategy effectively reduces energy emission from short, adjacent elements, thereby improving the radiation pattern clarity and efficiency. However, it introduces design complexities that require complicated feedline transpositions, potentially increasing cost and maintenance. In addition, the specificity of phase relationships and element spacing can limit flexibility in array configuration.

In this work, a novel antenna design with a distinct current distribution is realized using a straight connection configuration. In order to mitigate the potential performance degradation caused by same-phase currents within the elements, an optimized element spacing strategy is introduced that deviates from the traditional design rules of log-periodic dipole array antennas. As shown in Fig. 3, by carefully adjusting the element spacing to half the wavelength at different operating frequencies, the adjacent elements exhibit phase opposition. This phase reversal between adjacent elements results in a phase progression that enables end-fire beamforming. Similar to the crisscross connection approach, this innovative approach improves radiation performance while maintaining the versatility of the array configuration.

To guide optimal antenna design, an analysis of how variations in major parameters affect important antenna characteristics is conducted. Figs. 4(a) and (b) display the simulated results of $|S_{11}|$ and front-to-back ratio of the proposed antenna with different α values. The chosen value of $\alpha = 60^{\circ}$ for the proposed antenna demonstrates superior performance in terms of return loss and front-to-back ratio. Figs. 5(a) and (b) demonstrate that the distance L_1 between the ground plane and the bowtie dipole impacts the antenna's return loss and front-to-back ratio. $L_1 = 3.0$ mm is chosen for its superior front-to-back ratio performance. As per the effects of L_1 and α parameters, the antenna exhibits improved front-to-back ratio performance when $u = 1.2$, observable in Figs. 6(a) and (b). Based on the results shown in Fig. 7, it is evident that the return loss is significantly impacted by the value of v. In order to ensure adequate impedance bandwidth and electrical dimensions, a v value of 1.5 is selected for this design.

Based on the above antenna structure and parameter analysis results, a broadband bowtie-based log-periodic array antenna is designed and optimized by the High Frequency Simulation Software (HFSS). To improve the simulation accuracy, the discrete sweep type settings with a maximum number of passes of 15 and a maximum delta s of 0.02 were applied. Table 1 lists the final optimal parametric values for the proposed antenna. Fig. 8(a) shows the simulated results of the proposed antenna,

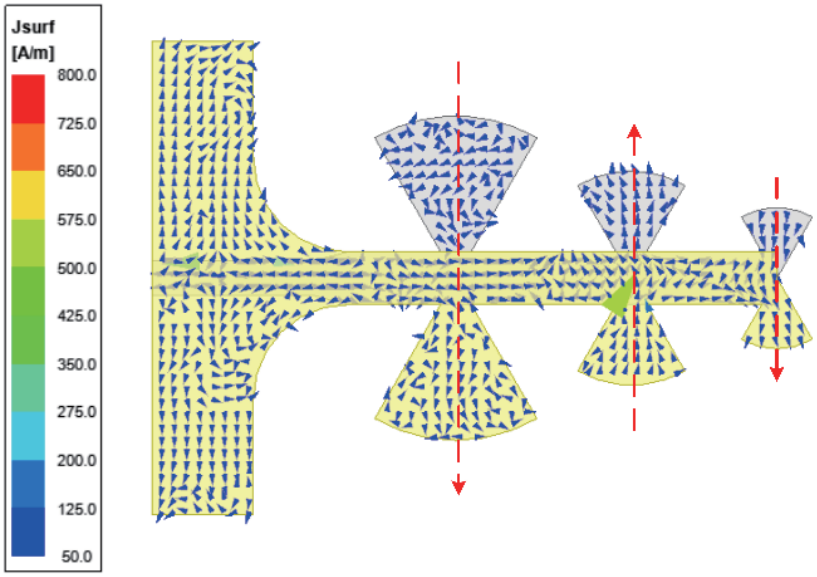

FIGURE 3. Electric field distribution of the proposed antenna at 28 GHz.

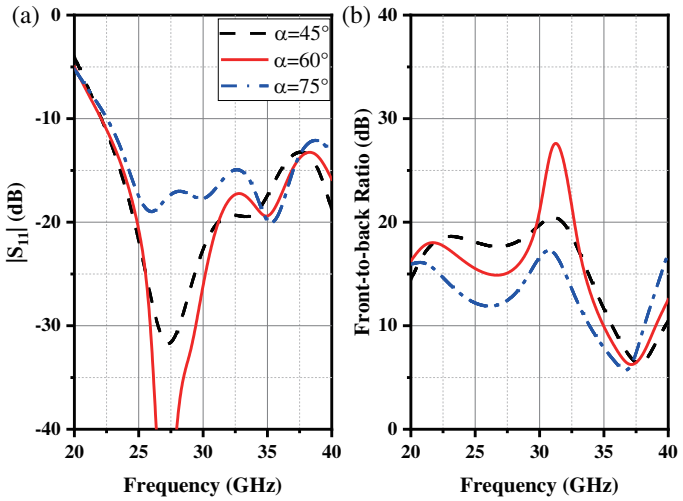

FIGURE 4. Simulated results versus the flare angle α. (a) $|S_{11}|$. (b) front-to-back ratio.

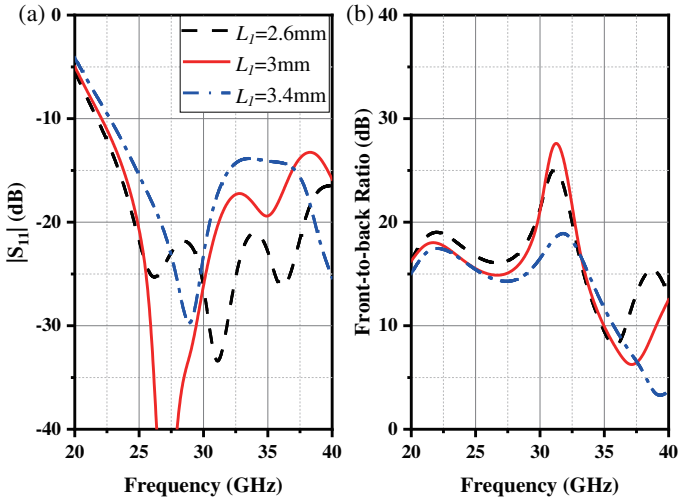

FIGURE 5. Simulated results versus the L_1. (a) $|S_{11}|$. (b) front-to-back ratio.

TABLE 1. Optimized dimensions of the proposed antenna.

Parameter	Value (mm)	Parameter	Value (mm)
W_c	0.06 mm	R_2	1.58 mm
W_m	0.52 mm	R_3	1.05 mm
W_p	0.78 mm	L_1	3 mm
d	0.025 mm	L_2	2.6 mm
R	1.4 mm	L_3	2.2 mm
$R1$	2.4 mm	α	60 deg
u	1.2	v	1.5

which shows that the return loss is less than 10 dB from 22.1 to 40 GHz. In addition, the antenna gain in the boresight direction is greater than 5 dBi from 24.1 to 34.8 GHz.

The microstrip line is used to feed the proposed antenna. However, it is not conducive to testing or integration with the system, and a CPW line is also needed. At the same time, a transition structure is used to realize broadband impedance matching between the microstrip line and CPW line. In this structure, the TGV is used to connect the ground plane between the M1 and M2 layers. Fig. 8(b) shows the simulated results of

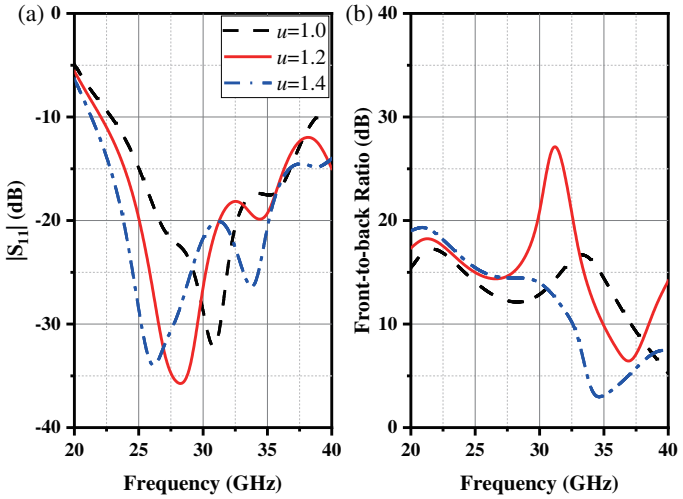

FIGURE 6. Simulated results versus the u. (a) $|S_{11}|$. (b) Front-to-back ratio.

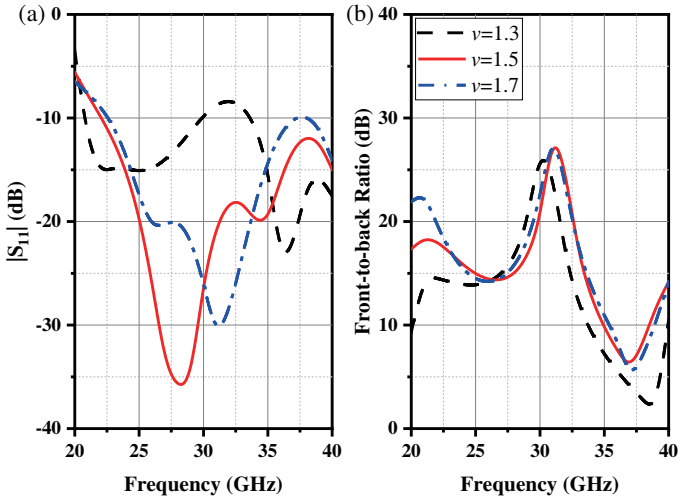

FIGURE 7. Simulated results versus the v. (a) $|S_{11}|$. (b) Front-to-back ratio.

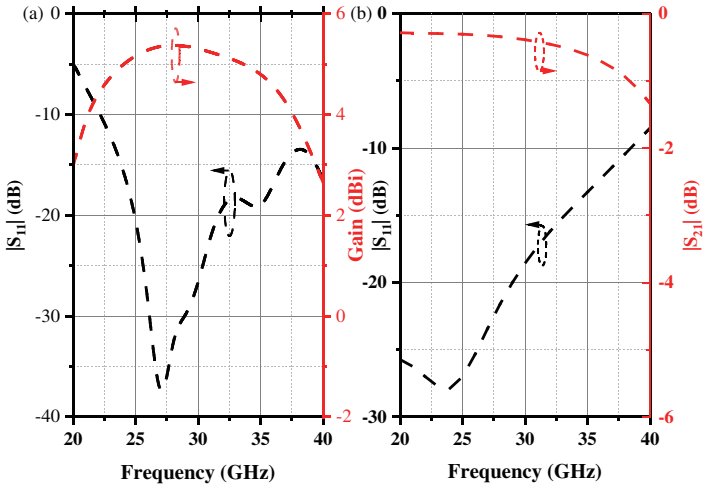

FIGURE 8. Simulated results. (a) Proposed antenna. (b) Transition structure.

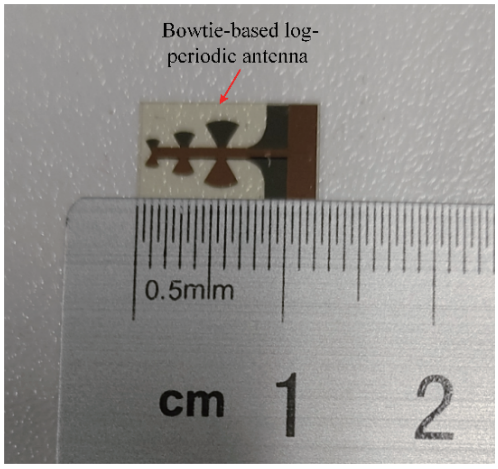

FIGURE 9. Photograph of the proposed antenna.

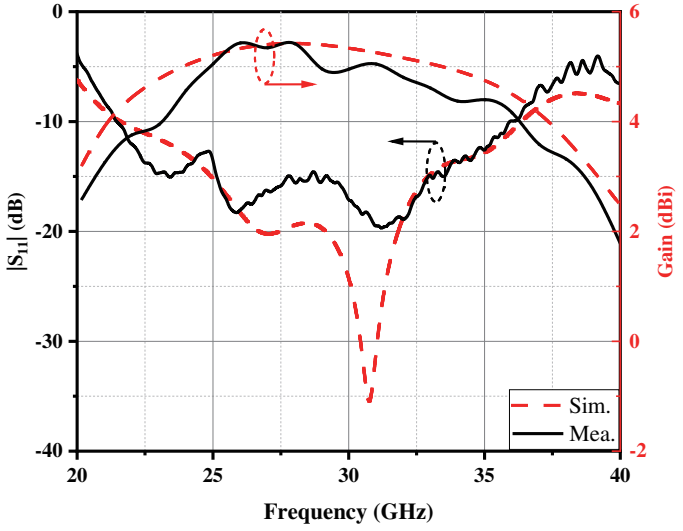

FIGURE 10. Measurement and simulation $|S_{11}|$ and Gain results of the proposed antenna.

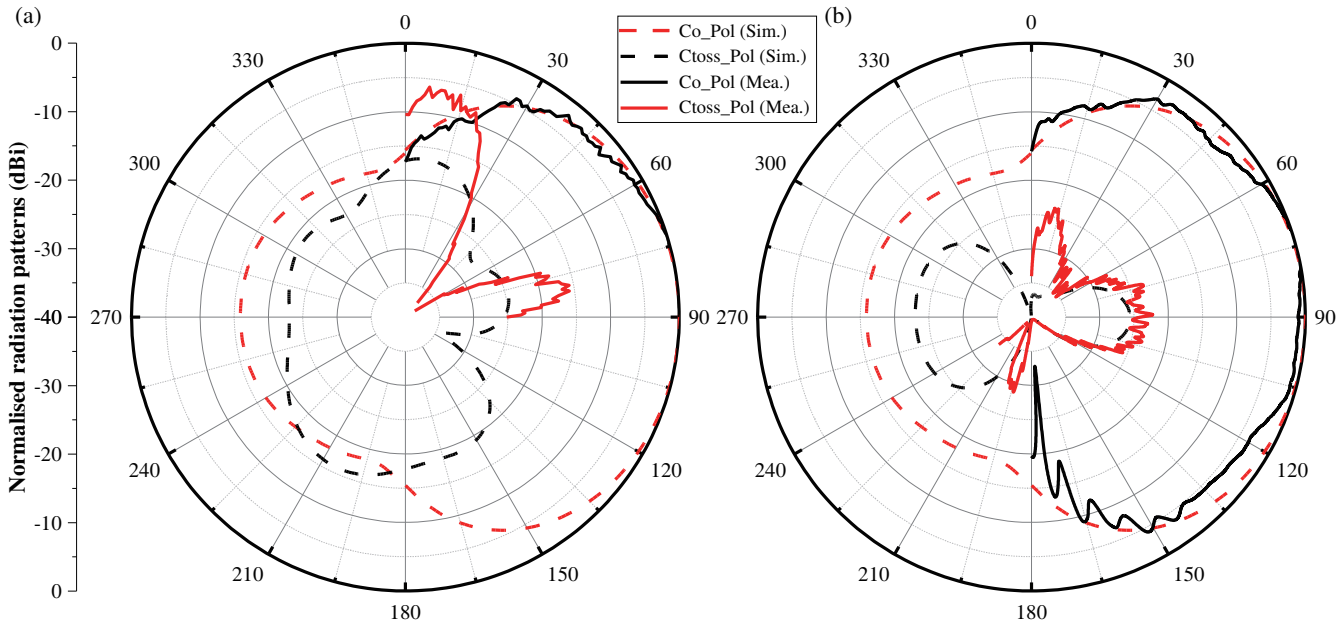

FIGURE 11. Measurement and simulation radiation patterns of the proposed antenna at 28 GHz. (a) E-plane. (b) H-plane.

TABLE 2. The performance comparison of the proposed 28 GHz glass antenna with the state-of-the-art results.

Ref.	Antenna Type	Frequency (GHz)	FBW (%)	Gain (dBi)	Size (λ_0)	Thickness (λ_0)
[9]	Ygai-Uda	21.9–29.8	28.2	4.6	0.34×0.40	0.28
[11]	Ygai-Uda	n.a.	31	9	n.a.	0.065
[13]	Monopole antenna with periodic patch director	24–30.7*	> 23.9	1	n.a.	0.42
[14]	Square loop antenna	23–28*	> 17.8	5	n.a.	0.084
[15]	1×4 series-connected patch array antenna	27.8–28.9	3.9	10	n.a.	0.033
This work	Bowtie-based log-periodic array antenna	21.536.1	52.1	5.63	1.12×0.65	0.028

*Beyond this rang.

the proposed transition structure; the 10 dB return loss bandwidth is from 20 to 38.5 GHz; and the insertion loss is less than 0.35 dB at 28 GHz. Since the operating bandwidth of the transition is smaller than that of the antenna, the achieved impedance bandwidth of the proposed antenna would be affected by the transition. However, the 28 GHz band (n257, n258, and n261 5G-NR FR2 bands) can still be covered.

4. MEASUREMENT RESULTS

To verify the performance, the proposed antenna is fabricated by GIPD process. Fig. 9 shows a photograph of the sample, and the total size of the proposed antenna is $12 \times 7\,\text{mm}^2$, about $1.12 \times 0.65\lambda^2$ (where λ is the free-space wavelength at 28 GHz). For accurate measurements, a probe-based antenna measurement setup is used in an anechoic chamber. Specifically, a 250 µm pitch air coplanar probe (ACP) is used to feed the antenna sample. A Keysight N5247B vector network analyzer (VNA) is used to measure the gain, return loss performance, and radiation pattern.

Figure 10 shows the simulated and measured $|S_{11}|$ and gains of the proposed antenna. As shown, the 10 dB impedance bandwidth is from 21.5 to 36.1 GHz. Notably, the measurement results agree well with the simulation. Using the gain comparison method, the proposed antenna gain is measured showing the gain higher than 4 dBi from 23 to 36 GHz, and its peak gain is 5.63 dBi at 28 GHz.

Based on the probe-based antenna measurement setup in an anechoic chamber, Fig. 11 shows E-plane (XY-plane) and H-plane (YZ-plane) co-polarization (Co-Pol) and cross polarization (Cross-Pol) radiation patterns at 28 GHz, respectively. Blocked by some parts of the measurement assembly, the E-plane cannot be measured within the whole angular range. The measured 3-dB beam width of the proposed antenna is about 37° and 41° in E- and H-planes at 28 GHz, respectively. And the cross polarization in both E- and H-planes is 20 dB less than the co-polarization.

Table 2 shows a performance comparison between the proposed antenna and the state-of-the-art results. The proposed antenna offers a wider bandwidth than the previous works in [9, 11, 13–15], covering the n257, n258, and n261 bands. This feature ensures reliable communication across a wide range of frequencies, making it highly suitable for 5G mm-wave applications that require high data rates and low latencies. Furthermore, the antenna maintains a stable gain, which is essential for ensuring consistent signal quality during transmission in mm-wave frequencies. Additionally, its low profile enables easy integration into various devices and systems to meet the varied communication requirements in mm-wave frequencies, in comparison to the previous works in [11, 13–15]. Therefore, the proposed antenna has a low profile, wide bandwidth, and stable gain, making it an attractive candidate for mass production of 5G mm-wave applications.

5. CONCLUSION

This paper presents a novel approach to meet the requirements of 5G mm-wave applications through the design and exploration of a broadband bowtie-based log-periodic array antenna. The antenna, implemented on a high dielectric constant glass substrate using the GIPD process, strategically arranges bowtie-based dipole elements to overcome radiation direction issues associated with conventional straight connections, providing a notable advantage in achieving a wide bandwidth. The paper further analyzes the effects of key parameter variations on antenna characteristics and introduces a feeding structure combining CPW to microstrip line and microstrip line to strip line. The optimized prototype antenna exhibits a 10 dB impedance bandwidth from 21.5 to 36.1 GHz and a gain exceeding 5.63 dBi, showcasing its potential suitability for 5G mm-wave applications.

REFERENCES

[1] Wang, X., L. Kong, F. Kong, F. Qiu, M. Xia, S. Arnon, and G. Chen, "Millimeter wave communication: A comprehensive survey," *IEEE Communications Surveys & Tutorials*, Vol. 20, No. 3, 1616–1653, 2018.

[2] Kausar, S., A. Kausar, H. Mehrpouyan, M. U. Hadi, and S. Tariq, "Comparative analysis of smart beam-steering antennas for mm-wave communication systems & 5G," *Progress In Electromagnetics Research B*, Vol. 98, 147–164, 2023.

[3] 3GPP. 5G NR Specs. Accessed: 2017. [Online]. Available: http://www.3gpp.org/DynaReport/38-series.html, Apr. 2022.

[4] Inomata, M., T. Imai, D. Kitayama, T. Sayama, O. Kagaya, H. Shoji, S. Takeuchi, K. Nobuoka, S. Itoh, H. Murai, A. Simonsson, and P. Okvist, "Downlink performance using vehicle glass mounted antenna for 28-GHz band in high mobility environment," in *2019 IEEE 89th Vehicular Technology Conference (VTC2019-Spring)*, 1–5, Kuala Lumpur, Malaysia, 2019.

[5] Perez, P., D. Corregidor, E. Garrido, I. Benito, E. Gonzalez-Sosa, J. Cabrera, D. Berjon, C. Diaz, F. Moran, N. Garcia, J. Igual, and J. Ruiz, "Live free-viewpoint video in immersive media production over 5G networks," *IEEE Transactions on Broadcasting*, Vol. 68, No. 2, 439–450, Jun. 2022.

[6] Jo, O., W. Kwon, and W. Hong, "Achieving 360° coverage dynamic and switchable beamforming through resource-efficient switchable antennas for future mmwave IoT devices," *IEEE Transactions on Industrial Electronics*, Vol. 68, No. 9, 8982–8991, Sep. 2021.

[7] Vaezi, M., A. Azari, S. R. Khosravirad, M. Shirvanimoghaddam, M. M. Azari, D. Chasaki, and P. Popovski, "Cellular, wide-area, and non-terrestrial IoT: A survey on 5G advances and the road toward 6G," *IEEE Communications Surveys & Tutorials*, Vol. 24, No. 2, 1117–1174, 2022.

[8] Kakutani, T., Y. Suzuki, M. Koh, S. Sekiguchi, S. Matsumura, K. Oki, S. Mishima, N. Ishikawa, T. Ogata, S. Erdogan, M. Ali, M. Kathaperumal, and M. Swaminathan, "Material design and high frequency characterization of novel ultra-low loss dielectric material for 5G and 6G applications," in *2021 IEEE 71st Electronic Components and Technology Conference (ECTC)*, 538–543, San Diego, CA, USA, 2021.

[9] Watanabe, A. O., T.-H. Lin, M. Ali, Y. Wang, V. Smet, P. M. Raj, M. M. Tentzeris, R. R. Tummala, and M. Swaminathan, "Ultrathin antenna-integrated glass-based millimeter-wave package with through-glass vias," *IEEE Transactions on Microwave Theory and Techniques*, Vol. 68, No. 12, 5082–5092, Dec. 2020.

[10] Zhang, J., S. Zhang, and G. F. Pedersen, "Wideband endfire on-glass array for 5G handset applications," in *2019 IEEE 90th Vehicular Technology Conference (VTC2019-Fall)*, 1–4, Honolulu, HI, USA, 2019.

[11] Wang, D., M. Nickel, P. Schumacher, E. Polat, H. Tesmer, R. Jakoby, and H. Maune, "A planar quasi yagi-uda antenna designed for liquid crystal based end-fire phased arrays," in *2021 IEEE Radio and Wireless Symposium (RWS)*, 164–167, San Diego, CA, USA, 2021.

[12] Xia, C., H. Wang, G. Wang, and X. Ming, "Advanced packaging of 3D fan-out RF microsystem for 5G IoT communication," in *2020 21st International Conference on Electronic Packaging Technology (ICEPT)*, 1–4, Guangzhou, China, 2020.

[13] Youn, S., D. Jang, N. K. Kong, and H. Choo, "Design of a printed 5G monopole antenna with periodic patch director on the laminated window glass," *IEEE Antennas and Wireless Propagation Letters*, Vol. 21, No. 2, 297–301, Feb. 2022.

[14] Gao, M., Y. Li, S. Yang, C. Wu, B. Tian, and J. An, "Wide band millimeter wave circular polarization antenna based on glass wafer substrate," in *2021 IEEE MTT-S International Microwave Workshop Series on Advanced Materials and Processes for RF and THz Applications (IMWS-AMP)*, 103–105, Chongqing, China, Nov. 2021.

[15] Chang, Y.-H., J.-C. Chen, W. Chung, W.-Y. Li, P.-T. B. Shih, A. Ng'oma, C. Yang, M.-C. Huang, H.-Y. Lin, C.-H. Wang, H.-T. Huang, and C. Kim, "A novel fabrication process and measurement results of a 28GHz glass antenna with single TGV for 5G communication applications," in *2019 14th International Microsystems, Packaging, Assembly and Circuits Technology Conference (IMPACT)*, 112–115, Taipei, Taiwan, Oct. 2019.

[16] "Schoot technology, af32 glass," https://www.schott.com/en-us/products/af-32-eco-p1000308, 2023.

[17] Balanis, C. A., *Antenna Theory: Analysis and Design*, John Wiley & Sons, 2016.